sustainability

MDPI

Article

Spatio-Temporal Dynamic Characteristics and Landscape Connectivity of Heat Islands in Xiamen in the Face of Rapid Urbanization

Ziyi Chen [1,2,3], Xiaoqian Lin [1,2,3], Mingzhe Li [1,2,3], Ye Chen [1,2,3], Yabing Huang [1,2,3], Yujie Zhu [1,2,3], Jiaxin Chen [1,2,3], Taoyu Li [4], Weicong Fu [1,2,3] and Jianwen Dong [1,2,3,*]

1 College of Landscape Architecture and Art, Fujian Agriculture and Forestry University, 15 Shangxiadian Rd., Fuzhou 350002, China; 3211726008@fafu.edu.cn (Z.C.); 1221775002@fafu.edu.cn (X.L.); 5221726036@fafu.edu.cn (M.L.); 2191775001@fafu.edu.cn (Y.C.); 2201775005@fafu.edu.cn (Y.H.); 2211775001@fafu.edu.cn (Y.Z.); 3211726003@fafu.edu.cn (J.C.); weicong.fu@fafu.edu.cn (W.F.)
2 Engineering Research Center for Forest Park of National Forestry and Grassland Administration, 63 Xiyuangong Rd., Fuzhou 350002, China
3 Wuyishan National Park Research Institute, 15 Shangxiadian Rd., Fuzhou 350002, China
4 Xiamen Tobacco Industry Co., Ltd., 1 Xinyang Rd., Haicang District, Xiamen 361000, China; lty23208@fjtic.cn
* Correspondence: fjdjw@fafu.edn.cn

check for updates

Citation: Chen, Z.; Lin, X.; Li, M.; Chen, Y.; Huang, Y.; Zhu, Y.; Chen, J.; Li, T.; Fu, W.; Dong, J. Spatio-Temporal Dynamic Characteristics and Landscape Connectivity of Heat Islands in Xiamen in the Face of Rapid Urbanization. *Sustainability* **2023**, *15*, 14603. https://doi.org/10.3390/su151914603

Academic Editors: Vincenzo Barrile and Matteo Gentilucci

Received: 20 July 2023
Revised: 1 October 2023
Accepted: 4 October 2023
Published: 9 October 2023

Abstract: With the acceleration of urbanization, urban heat waves have become a major problem affecting the lives of citizens. In this context, the accurate identification of the key patches and nodes of urban heat islands is important for improving the urban environment. This study examined the Landsat image data from Xiamen city in 2001, 2011, and 2021 to analyze the construction of the urban heat island (UHI) network. A morphological spatial pattern analysis (MSPA) and landscape connectivity model were utilized to identify the central thermal landscape patches and key nodes of UHI and their spatial and temporal evolution characteristics in the urban development process. The ultimate goal of this research is to provide valuable insights that can contribute to the enhancement of the urban environment. The results showed that (1) there was a significant increase in the heat island area (HIA) of Xiamen from 2001 to 2021, and the heat island patches show a concentrated trend. The temperature contrast between the urban area and the surrounding countryside was more distinct, indicating the urban construction land has a tendency to gather and spread. (2) The core area of the heat island accounted for the largest proportion of the thermal landscape area during the study period, and its proportion increased significantly. And the rate of increase was first rapid and then slow. The areas of the edge, branch, islet, bridge, loop, and perforation classes all showed different degrees of a decreasing trend. This indicates an increasing degree of aggregation between heat island patches. (3) The top 20 thermal landscape patches with high landscape connectivity importance values were identified. Among them, the importance value and area of the first four patches are relatively large, and belong to the three importance classes of extremely important, important, and generally important heat island core patches, which deserve focused attention and optimization. (4) Cooling measures can be prioritized for core areas of heat islands with high importance values. Connections between hot and cold islands can be interrupted or connected to mitigate the heat island effect throughout the region. The results of this study have important practical guidance for urban planning and sustainable development.

Keywords: heat island effect; morphological spatial pattern analysis; landscape connectivity; climate mitigation

1. Introduction

With accelerated global urbanization, rapid urban expansion has led to profound changes in land use patterns, which in turn have triggered structural and functional changes in urban ecosystems and led to a series of ecological and environmental problems [1–6]. Among them, the heat island effect has become a major problem affecting the urban environment and citizens' lives [7,8]. The increasing temperature differences between urban and suburban areas have exacerbated urban air pollution due to thermal circulation and have increased the chance of extremely severe weather [8,9]. On the other hand, high temperatures have a huge impact on residents' health and daily lives [10,11]. In this context, how to mitigate urban heat islands to promote sustainable social development and improve peoples' quality of life has gradually become a hot topic of research in urban ecology, landscape ecology, geography, and other multidisciplinary disciplines.

Due to the intensive development of remote sensing technology, the study of the urban heat island effect based on the land use landscape pattern has been widely used. Most studies have shown that the land use is a determinant of the urban heat island effect. Among them, urban impervious surfaces have the greatest impact on the surface thermal environment, and there is a positive correlation between the impervious surface area and surface temperature [12,13], while blue-green spaces such as forests and water bodies contribute to the mitigation of the urban heat island effect [14,15]. Specific to the landscape structure and configuration of different land morphology, some studies have shown that when the ecological land cover exceeds 70%, the cooling effect is relatively obvious. As for the effect of different land types on the temperature, it has [16] been pointed out that the impermeable surface patches located in surface urban heat island areas are complex in shape, high in density, large in area and also high in aggregation, thus enhancing local warming. Forest patches in the surface urban heat sink area also exhibit a complex shape, large area, and a high degree of aggregation, while playing a greater role in regional cooling [17]. However, recent urban heat island studies have focused more on the statistical analysis at the overall regional scale or simply at the patch level, which makes it difficult to reveal the thermal landscape pattern of urban heat island regions. It is difficult to apply the relevant research results effectively in practice because the role of the landscape networks is neglected.

In recent years, studies have mainly explored the urban heat island effect from the perspective of the landscape patches, such as the influence of the size, shape, composition, and type of patches on the urban heat island effect [18–22]. For example, Yu, Zhao-Wu et al. revealed the existence of an efficiency threshold for the optimal patch size to achieve the maximum cooling efficiency of the urban green space [23]. In addition, the influence of the spatial relationship between urban green spaces on the urban heat island effect has been explored. For example, Shih, Wan-Yu et al. suggest that spatially compact and well-connected green spaces provide better cooling for the adjacent urban areas than large individual green spaces [24]. However, the above cooling measures are mainly based on a simple patch-mosaic model concept, which can hardly reflect the overall pattern and connectivity of the urban heat island effect. Studies have focused on how to mitigate the heat island effect by increasing the regional connectivity of heat island patches, but there is a lack of research on mitigating the urban heat island effect from a network and overall connectivity perspective [25,26]. In this study, the morphological spatial pattern analysis (MSPA) method is applied to the study of urban heat island networks. The MSPA characteristics can be used to effectively analyze the structural types of urban heat island networks. Based on a comprehensive understanding of the connectivity and accessibility between the core network patches, mitigation of the urban heat island effect can be achieved through targeted reduction in the connections between key patches [27]. The proposed connectivity indices such as the integral index of connectivity (IIC) and the probability of connectivity (PC) allow for a more accurate evaluation of the landscape connectivity in the study area based on the landscape mapping theory. At the same time, the MSPA calculations can be used to identify the patches and corridors that are important for the maintenance of the landscape connectivity and prioritize them for optimization [27,28]. In addition, Xiamen's geographical location is unique in that, as a coastal city, it is able to mitigate the heat island effect by connecting a large area of cold islands [29].

Xiamen is a special economic zone in China, an important central city on the southeast coast, and a port and scenic tourist city that has won the UN Habitat Scroll of Honor Award. We should obtain a comprehensive understanding of the spatial pattern and network of heat islands within Xiamen's administrative boundaries, and formulate a scientific sustainable development plan. This has important implications for the development of all rapidly urbanizing regions. Based on this, this study analyzes the evolution characteristics of the urban heat island effect in 2001, 2011, and 2021 with Xiamen as the research objective. By introducing the MSPA and landscape connectivity index, this study analyzes the spatial and temporal evolution characteristics of the urban heat island network and further explores the key patches that influence the heat island network. Finally, the key points in the urban heat island network are clarified, so as to propose targeted measures to mitigate the urban heat island effect.

2. Materials and Methods

2.1. Study Area Overview

Xiamen (located between 24°23′ N and 24°54′ N, 117°53′ N and 118°26′ E) is an important port and scenic tourist city in the southeast coastal region of China, and is known as the "National Ecological Garden City". Xiamen has a subtropical maritime monsoon climate, which is warm and humid. The light and heat conditions are excellent and the rainfall is abundant. The average annual rainfall is around 1200 mm, with the most rainfall from May to August every year. The marine environment divides the city into 2 parts: Xiamen Island and the mainland. Xiamen Island contains Siming District and Huli District. The mainland consists of 4 jurisdictions (Jimei District, Haicang District, Tongan District, and Xiangan District). Xiamen's land use classification is shown in Figure 1 (the year of geographic coverage data is 2023). The overall topography slopes from northwest to southeast. The topography is dominated by coastal plains, terraces and hills. Over the past 30 years, Xiamen has been one of the fastest-growing cities in China. The urbanization rate of Xiamen is 88.33% and 90.1% in 2010 and 2021, respectively, ranking 6th among 45 key cities in China. The resident population of Xiamen in 2010 and 2021 was 3.56 million and 5.28 million, respectively. The average annual growth rate of the resident population is 3.87 percent (national: 0.53 percent). The urban population continues to grow. The urban population accounts for 89.41 per cent, while the rural population accounts for 10.59 per cent. Compared to 2010, the urban population has increased by almost 1.5 million and the rural population by about 130,000, with the urban population share increasing by 1.08 percent. During this period, the size of construction sites increased significantly. This exacerbated the frequency of extreme heat waves in the city, and residents experienced frequent hot weather as a result [30]. According to the Xiamen Meteorological Station, the extreme maximum temperature in Xiamen in 2022 was 38.2 °C, 0.8 °C higher than normal. In 2022, there were a total of 19 stations in the city where the extreme maximum temperature was ≥40 °C, with a maximum of 41.1 °C. The maximum temperature in Xiamen was 41.1 °C in 2022. Since the 21st century, the extreme maximum temperatures in and around Xiamen island are higher than normal. At the same time, the annual cumulative number of high temperature days (daily maximum temperature ≥ 35 °C) for 44 days, 2.6 times the normal year, since 1956 for the history of the third most. The number of high-temperature days in Xiamen has been significantly higher than normal since the 21st century. And there were large spatial differences in the distribution of the number of hot days across regions. While some peri-urban regions had no hot days ≥ 35 °C, some urban regions had 71 hot days. Therefore, in order to provide urban planners with strategies to effectively mitigate the heat island effect, it is particularly important to explore research on how to effectively cool down the temperature.

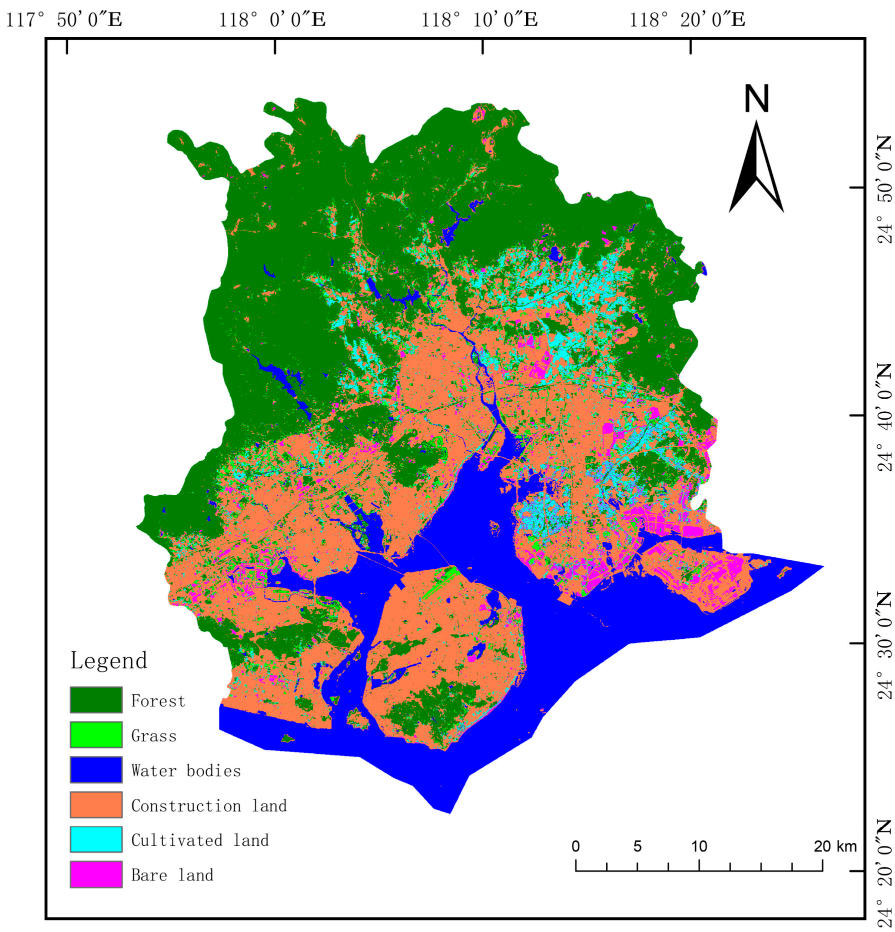

Figure 1. Geographic location and land use classification of the study area.

2.2. Data Sources and Pre-Processing

Due to the rainy summer in Xiamen, some of the summer Landsat data cannot meet the requirement of less than 10% cloud cover range. Therefore, this study takes different stages of urban development in the study area as the nodes, and selected Landsat image data (line number 43/strip number 119) from 12 September 2001, 16 September 2011 and 25 July 2021 with a cloud cover range less than 10%. The above data is from the USGS website (https://earthexplorer.usgs.gov/, accessed on 22 March 2023). The above data were obtained from the USGS website (https://earthexplorer.usgs.gov/, accessed on 22 March 2023). The study area boundaries refer to the site plan of the Xiamen City General Urban Plan (2011–2020), from the Xiamen Natural Resources and Planning Bureau (http://zygh.xm.gov.cn/, accessed on 30 March 2023). First, the multispectral bands and infrared bands of Landsat images were preprocessed with radiometric calibration, cropping, and atmospheric correction using ENVI 5.3 software. Then, the land surface temperature (LST) is obtained by inversion, and the atmospheric correction method (also called radiative transfer equation (RTE)) is used to convert the original image element brightness values of the thermal infrared band images to the true temperature values of the surface features (band 6 for Landsat ETM+ and band 10 for Landsat OLI/TIRS) [31–33].

2.3. Image-Based Surface Temperature Inversion

In this study, after comparing the commonly used algorithms such as mono-window algorithm, universal single-channel algorithm, radiative transfer equation (RTE) and split-window algorithm, the most commonly used RTE algorithm was chosen. RTE is one of the earliest-developed surface temperature inversion algorithms. The basic idea of this algorithm is based on the thermal infrared radiation transport equation to remove the influence of the atmosphere on thermal radiation in the process of radiation transport, so as to obtain the surface temperature more accurately. RTE has a wide range of applicability, and it can be applied to thermal infrared remote sensing data from any sensor. Moreover, RTE has a solid physical foundation and high inversion accuracy. The algorithm assumes a consistent atmospheric influence in clear weather and small areas. It is therefore insensitive to radiometric errors due to atmospheric influences [34]. Meanwhile, it has been shown that compared with other algorithms, RTE can achieve the highest accuracy in environments with high atmospheric water vapor content, which is more suitable for application in subtropical rainy and humid cities [23]. Therefore, RTE is selected for this study.

The LST inversions for this study were performed in ENVI 5.3, and the RTE was calculated as follows:

$$L_\lambda = [\varepsilon B(T_s) + (1-\varepsilon) L \downarrow]\tau + L\uparrow, \tag{1}$$

where ε is the surface specific emissivity, Ts is the true surface temperature (LST) in K (Kelvin), B(Ts) is the blackbody thermal radiance, and τ is the atmospheric transmittance in the thermal infrared band.

Using Equation (2), the LST is calculated as:

$$T_s = \frac{K_2}{ln\left(\frac{K_1}{B(T_s)+1}\right)}, \tag{2}$$

where, for TM, K1 = 607.76 W/($m^2 \times \mu m \times sr$) and K2 = 1260.56 K; for ETM+, K1 = 666.09 W/($m^2 \times \mu m \times sr$) and K2 = 1282.71 K; for TIRS Band10, K1 = 774.89 W/($m^2 \times \mu m \times sr$) and K2 = 1321.08 K.

2.4. Surface Temperature Classification

In order to visually compare the surface thermal environment of the study area in different periods and avoid the effects of errors in the inversion results, the LST values were first standardized. The heat island areas and non-heat island areas were classified by comparing the quantitative relationship between the standardized LST of a given raster, the average LST, and the standard deviation of temperature. The specific division method is as follows:

$$T_s = \frac{T_i - T_{\min}}{T_{\max} - T_{\min}}, \tag{3}$$

The standardized surface temperature values are graded, and the classification criteria are shown in the Table 1 [35]. In this study, the high-temperature and sub-high-temperature areas above the average temperature were combined as the heat island areas and used as the foreground data for the MSPA analysis. The rest of the temperature classes were combined as non-heat island areas as background data for MSPA analysis.

Table 1. Ranking of land surface temperature (LST) levels.

Grade	Division Standard
High-temperature zone	Ts > (a + 2std)
Sub-high-temperature zone	(a + 0.5std) < Ts ≤ (a + 2std)
Normal-temperature zone	(a − 0.5std) < Ts < (a + 0.5std)
Sub-low-temperature zone	(a − 2std) ≤ Ts < (a − 0.5std)
Low-temperature zone	Ts < (a − 2std)

Ts: standardized land surface temperature; a: mean standardized land surface temperature; std: standard deviation.

2.5. MSPA-based Thermal Landscape Element Identification

MSPA is a processing method based on mathematical morphology to classify binary image pixels and can be applied to digital images of any size and application area. The basic operations of the MSPA include the following: binary corrosion and expansion, binary open and close operations, skeleton extraction, and limit corrosion. The basic idea is to use structural elements with a certain morphology to measure and segment the spatial pattern in the image in order to achieve the purpose of image analysis and recognition. It is characterized by the ability to simplify image data, retain its basic shape and structural characteristics, categorize it appropriately, and remove the irrelevant structures [36]. The method extracts areas with landscape connectivity significance from the level of image elements as core areas, placing a clear emphasis on the structural connectivity [28,37]. Most of the previous relevant studies based on the MSPA model relied on land use data. In these studies, land use types were reclassified. The important natural ecological elements (specific land use types) were then extracted as the foregrounds, while the other land use types were used as the backgrounds. Finally, the MSPA analysis was performed using the Guidos analysis software to classify the foreground into seven basic pattern classes by morphology. In this study, the MSPA classification model is applied to the study of the urban heat island. According to the needs of the MSPA method, the surface temperature classification results were firstly converted into binary TIFF data with a spatial resolution of 30 m through ArcGIS. The surface temperature classification results were opened in ArcGIS, the heat island areas were reclassified as foreground for the MSPA analysis and the non-heat island areas were reclassified as background, and saved in Tiff format. Then, the above files were imported into the Guidos Toolbox software. According to the previous research results and the comparison of the multiple parameter experiments, the 8-neighborhood analysis method was adopted, and the edge width was set to 1 [27,28,37]. The method applies a sequence of morphological operators known as erosion, dilation, and anchored homotopic skeletonization. The erosion operator shrinks the objects, the dilation operator grows them, and the anchored homotopic skeletonization iteratively removes the boundary pixels of an object until the object is depicted by its line representation or skeleton. A logical sequence of these operations allows classifying the original binary image into a pixel-level map of up to nine mutually exclusive thematic classes describing the geometric features of the foreground mask [38]. After the above series of mathematical operations, seven basic pattern classes without overlapping each other were obtained: core, edge, branch, islet, bridge, loop, and perforation (Table 2) [36,39], and the results were counted.

Table 2. Definition of MSPA classes and their meaning in the urban heat island context.

Class	Meaning in the Urban Heat Island Context
Core	Core is defined as those urban heat island pixels whose distance to the non-urban heat island areas is greater than the given edge width.
Bridge	Bridge is defined as the sets of contiguous non-core heat island pixels that connect the ends of at least two different core areas. Bridges correspond to structural connectors or corridors that link different urban heat island core areas.
Islet	Islet is defined as the isolated urban heat island patches that are too small to contain core pixels.
Loop	Loop is similar to bridges but with the ends of the element connected to different parts of the same core heat island area.
Edge	Edge is defined as a set of urban heat island pixels whose distance to the patch edge is lower than or equal to the given edge width and corresponds to the outer boundary of a core area.
Perforation	Perforation is similar to an edge but corresponds to the inner boundary of a core heat island area.
Branch	Branch is defined as the pixels that do not correspond to any of the previous six categories. It typically corresponds to an elongated set of consecutive urban heat island pixels that emanate from an urban heat island area and do not reach any other urban heat island area at the other end.

2.6. Distance Threshold Setting and Landscape Connectivity Index Calculation

Landscape connectivity refers to the extent to which the landscape facilitates or impedes ecological flows [39]. Maintaining a good connectivity contributes to the stability of the ecosystem [40]. Currently, the integral index of connectivity (IIC), probability of connectivity (PC), and patch importance index (dI) are often used to reflect the level of landscape connectivity and the importance of the patches to landscapes as important indicators of the landscape pattern and function [28,29,41]. In this paper, we treat the surface thermal environment of the study area as a thermal landscape. If the impact of removing the specific urban heat island patches on the thermal landscape connectivity can be quantified, the location of the important patch nodes can be pinpointed. Then, measures can be taken to destroy the level of the thermal landscape connectivity and the regional urban heat island effect can be effectively mitigated. Therefore, we extracted the core area from the seven basic pattern classes obtained from the MSPA calculations as the heat landscape source sites by ArcGIS. Then, we used Conefor sensinode2.6 software to calculate the landscape connectivity indices IIC, PC, and dI to evaluate the connectivity level of the regional surface urban heat island [28]. And by comparing the changes of the correlation index values under 16 groups of distance thresholds of 100 m and 200~3000 m (with a gradient set at every 200 m), the best distance threshold for this study was determined. The IIC, PC, and dI are specifically calculated as follows:

$$\text{IIC} = \frac{\sum_{i=1}^{n}\sum_{j=1}^{n}\left(a_i a_j/1 + nI_{ij}\right)}{A_L^2}, \tag{4}$$

$$\text{PC} = \frac{\sum_{i=1}^{n}\sum_{j=1}^{n} a_i a_j p_{ij}^{*}}{A_L^2}, \tag{5}$$

$$\text{d}I(\%) = \frac{I - I_{remove}}{I} \times 100\%, \tag{6}$$

where n represents the total number of patches in the landscape, a_i and a_j represent the area of patch *i* and patch *j* in turn, nl_{ij} represents the number of connections between patch *i* and patch *j*; $P_{ij}{}^*$ represents the maximum value of the probability product of pathways between patch *i* and patch *j*, A_L is the total area of the landscape study area; I is the connectivity index value when there are landscape elements in the landscape, I_{remove} is the index value after removing the landscape element (e.g., after the disappearance of a heat island patch). When $0 \leq \text{IIC} \leq 1$ and the value of IIC is 0, it means that there is no connection between the heat island patches. When IIC is equal to 1, it means that the whole landscape is a heat island patch. When $0 \leq \text{PC} \leq 1$, a larger PC value represents a greater degree of plaque connectivity. The structural importance of the patches was characterized by measuring the relative change rate dI of the connectivity index values, after the disappearance of each patch. Higher dl values indicate that the nodes are more important for the landscape connectivity, which is crucial for regional surface heat island mitigation studies. The importance values calculated for each patch will differ by choosing different types of connectivity indices I. The variables I selected in this paper are PC and IIC, denoted by dPC and dIIC, respectively.

In this study, the 20 urban heat island source sites with the highest importance of patch connectivity in each year were selected based on the results of the IIC and PC importance calculations. And the importance of the urban heat island patches in the core area is visualized. Based on the natural intermittent classification, these urban heat island patches were classified into five classes: extremely important, important, generally important, less important, and unimportant [27].

3. Results and analysis

3.1. Spatial and Temporal Characteristics of Surface Temperature

As can be seen from Figure 2, the initially fragmented and scattered high-temperature areas and sub-high-temperature areas gradually tended to become densely distributed in patches during the period 2001–2021. In 2001, the normothermic zone was the most widely distributed. Only a very small area of small patchy areas existed in the high-temperature zone. The secondary high-temperature zone, on the other hand, was mainly scattered in patches in the study area, with relatively concentrated distribution in Xiamen Island

and the southeast region. In 2011, the high- and secondary high-temperature areas were significantly expanded and more aggregated in their distribution, and the expansion area was dominated by the coastal region. The sub-low- and low-temperature zones were mainly distributed in the northern mountains and southern waters. In 2021, the distribution of the high-temperature zones decreases significantly. The sub-high-temperature zone increased significantly and became more concentrated in the eastern and southwestern parts of the city. The sub-cold-temperature zone and low-temperature zones expanded in the north. The changes in the surface temperature over time indicate that the temperature difference between the main urban area of Xiamen and the surrounding countryside is becoming more and more pronounced. In this study, the high surface temperature zone and the sub-high temperature zone were extracted as the urban heat island area. By comparing the interannual variation of the urban heat island area, it was observed that the heat island area was increasing in two specific areas in the east and southwest of the city. These two areas are precisely the most rapidly developing key urban construction areas, while the heat island patches in other areas are shrinking and disappearing.

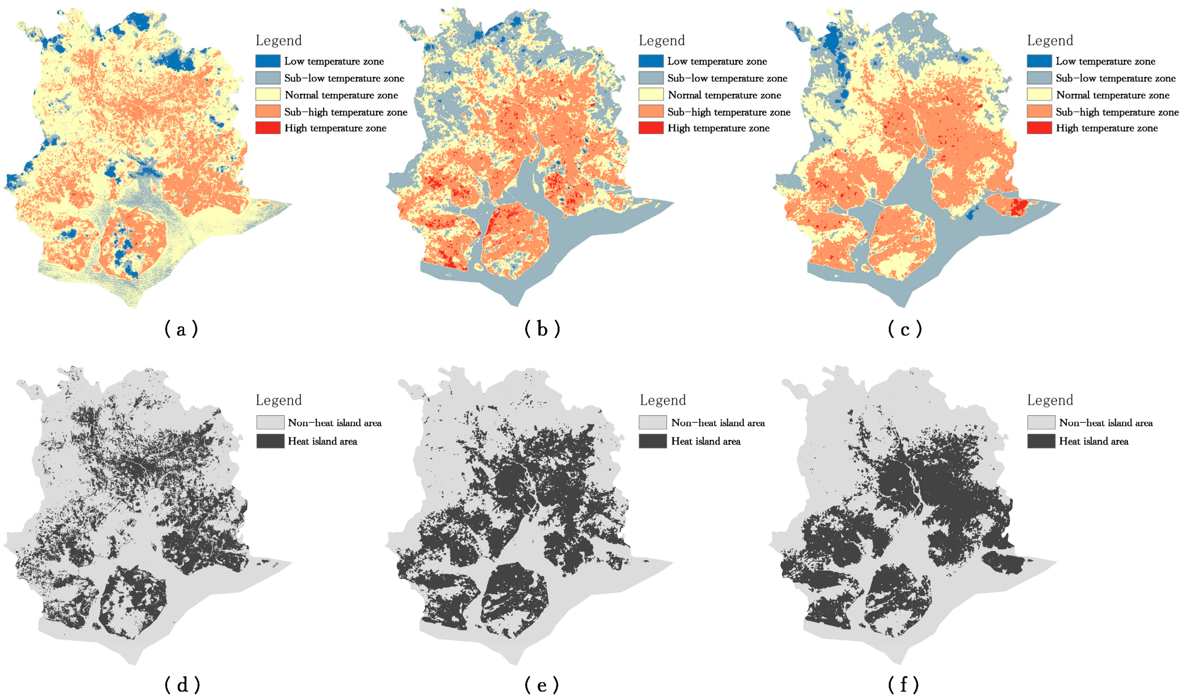

Figure 2. Urban surface temperature classification and heat island area classification from 2001 to 2021. (**a**) Surface temperature classification for 2001; (**b**) surface temperature classification for 2011; (**c**) surface temperature classification for 2021; (**d**) regional classification of heat islands in 2001; (**e**) regional classification of heat islands in 2011; (**f**) regional classification of heat islands in 2021.

3.2. Extraction of Structural Features of Urban Heat Island Distribution Based on MSPA

The spatial and temporal distribution pattern of urban heat island based on the MSPA from 2001 to 2021 is shown in Figure 3 and Table 3. The results show that the core area occupies the largest area. The core area in 2001, 2011, and 2021 is 357.20 km^2, 585.78 km^2, and 620.31 km^2, respectively: 65.91%, 87.05%, and 89.43% of the total area of heat island patches, respectively. The interannual variation in the area and proportion indicates a rapid increase in the core area during the period 2001–2011 and a slow increase during the period 2011–2021. The proportion of this type in the overall urban heat island patch has been showing an increasing trend. The spatial distribution of the core area showed a clear concentration to the east and southwest. The edge area is the type of area second only to the core area, with a gradually decreasing percentage of its area (20.97%, 8.02%, and 6.40%, in that order). This situation may occur because the edge areas usually surround the core areas, so the morphological distribution of the core areas will significantly influence the trend of the area change in the edge areas. The third and fourth in the MSPA classification are the perforation and branch areas, with area shares of 3.72%, 4.10%, 3.25%, and 4.16%, 0.45%, 0.51%, in that order. The former increases and then decreases. The latter shows an overall decreasing trend as time goes on. The area proportions of the heat island patches accounted for by the islet, loop, and bridge areas are all relatively small. Among them, the bridge area is the smallest type of area (the proportion of the area is 1.64%, 0.08%, and 0.11%, in that order). The area share of the islet areas decreased more significantly due to the tendency of the heat island patches to aggregate, with decreases of 2.06%, 0.17%, and 0.13%, in that order. The proportion of the area of the loop area shows a decreasing trend with the change in the core area pattern, which is 1.08%, 0.13%, and 0.16%, in that order. The combined results show that the core type occupies the majority of the heat island area in the MSPA model classification and has a significant influence on the remaining types, which is an important factor in determining the stability of the urban heat island network.

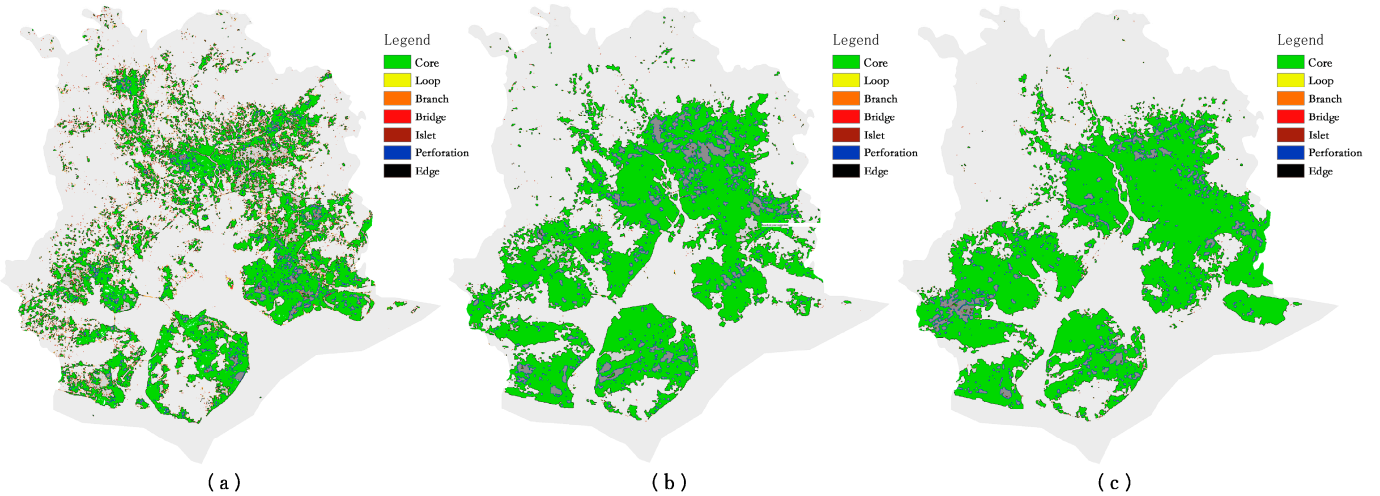

Figure 3. Results of MSPA-based urban heat island patch classification from 2001 to 2021. (**a**) 2001; (**b**) 2011; (**c**) 2021.

Table 3. Classification and statistical results based on MSPA.

Type	Area of 2001 (km^2)	Area Proportion of Urban Heat Island (%)	Area of 2011 (km^2)	Area Proportion of Urban Heat Island (%)	Area of 2021 (km^2)	Area Proportion of Urban Heat Island (%)
Core	357.20	65.91%	585.78	87.05%	620.31	89.43%
Edge	113.66	20.97%	53.99	8.02%	44.40	6.40%
Branch	22.57	4.16%	3.05	0.45%	3.56	0.51%
Islet	11.17	2.06%	1.11	0.17%	0.92	0.13%
Bridge	8.87	1.64%	0.53	0.08%	0.74	0.11%
Loop	5.83	1.08%	0.86	0.13%	1.14	0.16%
Perforation	20.18	3.72%	27.57	4.10%	22.55	3.25%

3.3. Establishment of Distance Thresholds for Landscape Connectivity

As shown in Figure 4, when the distance threshold is 100~400 m, the number of components (NC) between the centers of the thermal networks in the study area decreases rapidly with the increasing distance threshold. This suggests that the distance threshold is unsuitable for describing the connectivity status of the thermal networks in the region within this interval. When the distance threshold is 400~3000 m, the range of the NC value is relatively suitable and the change in the number of links (NL) value is relatively stable, which is a suitable distance threshold range. Then, the equivalent connectivity (EC) values of the IIC and PC, i.e., EC(IIC) and EC(PC), are combined with the change in the distance threshold. When the distance threshold is less than 1000 m, the two indices grow significantly. When it is greater than 1000 m, the change in the two indices tends to flatten out, and finally, the distance threshold of connectivity of this study landscape is determined as 1000 m.

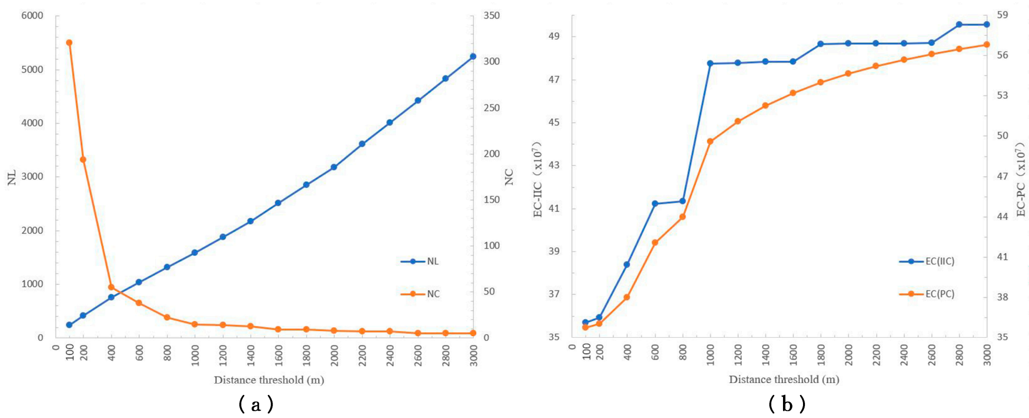

Figure 4. Variation of NC, NL, EC(IIC) and EC(PC) values with distance threshold at the center of the thermal landscape network. (**a**) NC and NL. (**b**) EC(IIC) and EC(PC).

3.4. Results of Landscape Connectivity Analysis

The importance ranking of the heat island patches in the core area based on landscape connectivity during the period 2001–2021 is shown in Figure 5. The spatial and temporal dynamics of the top 20 patches in terms of the importance value and their specific values are shown in Figure 6 and Table 4. In terms of the spatial distribution, the extremely important and significant core areas of Xiamen in 2001 were mainly distributed in the urban area of Xiamen Island and the major town clusters. The results of the dIIC and dPC values show that the importance of the connectivity of the patches is more balanced in this period compared to 2011 and 2021, with the first patch having a greater importance of connectivity compared to the other patches. In 2011, the very important core area developed rapidly in the central and western parts of Xiamen, connecting with the major town clusters and gradually forming a network. The very important core area was distributed on Xiamen Island in the south. The importance of the first four patches in Table 4 for that period was greater, and the first ranked patch had a much greater importance value than the other patches. In 2021, the very important core area expanded in all directions from that of 2011, the area of the western and eastern regions expanded significantly, and the distribution gradually tended to gather. The important core area continued to develop from Xiamen Island to the western part of the island. The connectivity was calculated for all the core area patches in that year, and it was found that the first four patches had large values of connectivity importance, and the first and second patches had extremely large values. As a whole, the importance of the head patches among the top 20 patches is increasing, and the proportion of the area they occupy is getting larger and larger. Meanwhile, the remaining thermal landscape patches are becoming less and less important, and the area of the patches is getting smaller and smaller, indicating that the head patches have a greater influence in urban planning and development. Therefore, it is significant to further take effective and appropriate measures for them first to alleviate the urban heat island.

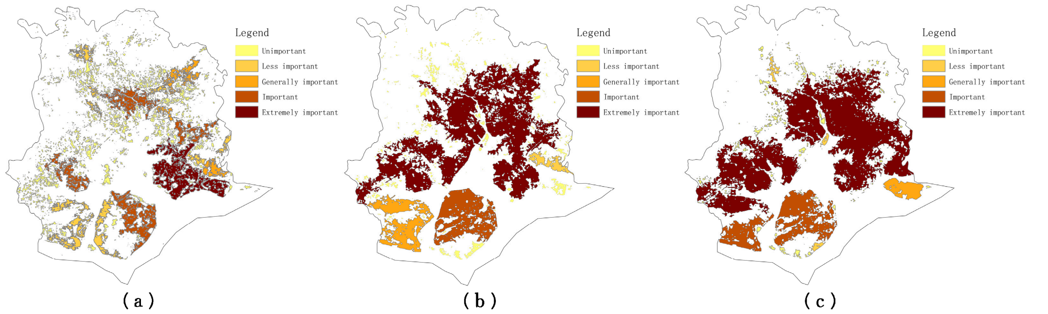

Figure 5. Classification of the importance level of urban heat island core patches. (**a**) 2001; (**b**) 2011; (**c**) 2021.

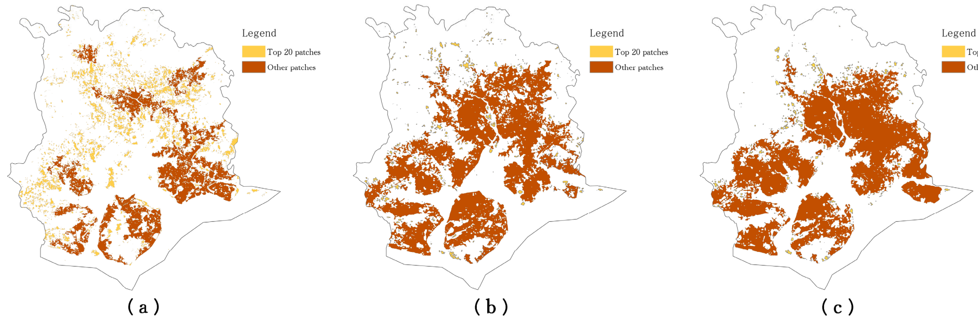

Figure 6. Spatial-temporal dynamics of the top 20 patches (**a**) 2001; (**b**) 2011; (**c**) 2021.

Table 4. Calculation results of the importance index of the top 20 patches in Xiamen from 2001 to 2021.

Sort	2001		2011		2021	
	dIIC (%)	**dPC (%)**	**dIIC (%)**	**dPC (%)**	**dIIC (%)**	**dPC (%)**
1	45.51	47.87	93.08	93.42	80.57	79.13
2	16.01	10.09	16.49	19.67	46.31	47.27
3	13.01	19.97	7.83	12.97	16.53	18.03
4	10.74	27.73	5.97	13.21	12.67	12.69
5	10.72	7.13	2.85	3.93	4.86	5.67
6	10.25	22.31	0.55	0.94	0.98	1.06
7	7.67	11.82	0.53	0.68	0.35	0.51
8	6.96	17.97	0.53	0.68	0.32	0.43
9	5.53	7.79	0.33	0.52	0.26	0.41
10	3.79	3.20	0.31	0.64	0.19	0.37
11	3.42	4.90	0.27	0.41	0.13	0.23
12	3.27	4.22	0.20	0.62	0.13	0.25
13	2.70	1.33	0.20	0.30	0.13	0.17
14	2.62	2.44	0.18	0.38	0.11	0.16
15	2.30	3.14	0.18	0.25	0.11	0.27
16	2.15	4.18	0.17	0.21	0.10	0.10
17	2.10	3.16	0.16	0.27	0.10	0.14
18	1.94	2.06	0.16	0.40	0.10	0.10
19	1.57	6.16	0.15	0.25	0.08	0.14
20	1.50	2.40	0.15	0.18	0.08	0.13

4. Discussion

4.1. Analysis of the Spatial and Temporal Evolution of the Heat Island of Xiamen

Dramatic changes in the surface temperature in Xiamen occurred in the period 2001–2021. Meanwhile, as the core area of the heat island increased significantly and the perforation area expanded slowly, the area of the remaining five kinds of patches all decreased significantly. The spatial pattern of heat islands tends to be concentrated in patches from the original fragmentation. From 2001 to 2011, with the rapid expansion of Xiamen's urban development area, the urban spatial structure was transformed from a "multi-core and single-center urban structure" as proposed in the "Xiamen City Master Plan (1995–2010)" to a "one-center, two-ring, one-main, four-supporting, and eight-slice urban spatial structure" as proposed in the "Xiamen City Master Plan (2004–2020)". The construction land increased significantly. Dramatic changes in the urban heat island pattern were produced. The core area of the heat island expanded dramatically, the center of gravity shifted to the southern coastal region, and the spatial distribution rapidly became concentrated from fragmentation. From 2011 to 2021, the overall urban pattern of Xiamen was transformed into what was proposed in the "Xiamen City Urban Master Plan (2011–2020)", which was approved and implemented in 2016: "a grouped bay city with 'one island, one belt and many centers'", increasing the construction and development within and around the key areas from 2011. Therefore, compared to the previous phase, the spatial pattern of the heat island changes were relatively moderate. The core area of the heat island grew slowly. The spatial distribution was more dense, mainly showing the shrinking of the perforation area and the islet area. The approach chosen for this study starts with the analysis of the network morphology of the urban heat islands, as opposed to the direct approach from a plaque perspective. In an urban heat island network, each heat island patch has a different relative location, connecting role, and importance. Raising the perspective of the study to the entire heat island network, the key patches that build and sustain the current heat island network can be identified after numerically analyzing the patches and corridors in the network by means of a landscape connectivity model. The research results based on heat island patches (e.g., land use type area thresholds, urban landscape pattern optimization) can be applied to these key patches, thus forming a closed loop of research from network to patches, making the whole research more comprehensive and of a higher practical application value.

4.2. Urban Space Optimization Strategy Based on Thermal Landscape Connectivity Analysis

Many studies related to urban heat islands have chosen to cut into the research from the perspective of the landscape patches. These studies investigate the impact of the patch composition and configuration on the urban heat island effect, and find the optimal solution to achieve the best mitigation effect on the urban thermal environment. These studies have proposed a number of effective mitigation measures, such as the optimal shape and size of the greenfield patches that can mitigate the urban heat island effect, and the spatial configuration of the greenfield areas that can achieve optimal cooling efficiency. However, before implementing these mitigation measures, it is clear that the most important step is to identify the key areas where the best mitigation benefits can be realized. This will allow for better integration of the thermal mitigation measures with urban planning. Previous studies by Yu Zhaowu et al. have shown that the urban heat island patches can be regarded as a "thermal" landscape [42]. They also proposed a new method for integrating the MSPA from a graph perspective. Their study demonstrated that a graph-based approach (e.g., MSPA) can be applied to segment a raster "thermal" landscape binary map (i.e., heat island versus non-heat island areas) into different landscape pattern categories to further identify the crucial heat island patches [27]. They then proposed a reverse thinking process. It was shown that in the reverse thinking process, urban heat island connectivity decreases when the links and pinch points are blocked to break the networks, thus significantly alleviating the urban heat island effect [43]. In order to achieve the precise location of key patches, a combination of MSPA analysis and landscape connectivity analysis is chosen in this paper. In the past, this method was mostly used for the establishment of habitat ecological networks. This method identifies the core area basic pattern classes of certain ecological significance in the study area and interconnects gradually fragmented habitat patches to produce a complete ecological network [28,44,45]. This method is now applied to urban heat island research. The focus is on finding and destroying the most critical patches in the original heat island network, blocking the structural connection of the heat island network, and connecting it to the cold island to effectively mitigate the urban heat island effect [29,46].

The results show that the extremely important urban heat island patches between 2001 and 2021 were mainly located in the central urban area of the study area and were increasing in size with more complex connections between patches. Based on the understanding of the current status of the urban heat island network in 2021, corresponding suggestions can be made on how to mitigate the heat island effect in Xiamen, which can be better integrated with urban design and planning. Based on the results, the central part of the city should be the focus of renovation. To improve the overall thermal environment optimization efficiency, measures can be prioritized for the patches ranked in the top three importance values. From the development plan of the whole city, we know that the central part of Xiamen vigorously promotes the development of the town. It is put into construction faster as an industrial, residential, and commercial center. The artificial building surface increases significantly. Combined with the experience and conclusions of a large number of previous studies, it is important to avoid a concentrated distribution of the heat source areas within the central area patches. The current land use structure within the heat island patches could be improved through the placement of green spaces or water bodies; small, irregularly shaped heat sink patches are set up to enhance surface heat exchange and help absorb the heat generated during city operations [9,47–50]. In addition, due to the advancement of many projects in the southern industrial park, in order to avoid further extension of the urban heat island patches to the south, the intensive use of construction land in the heat source patches can also be enhanced, while further encouraging the expansion of above-ground and underground space. In addition, it is also more feasible to increase the proportion of ecological land in the non-construction land area around these key heat island patches to achieve the construction and enhancement of the blue-green landscape. By blocking the pathway of heat flow and reducing the heat absorption, the heat island effect can be suppressed [47,49,51].

5. Conclusions

Based on the LST calculated by inversion, an MSPA was applied to delineate the functional types of the regional connectivity in the heat island, and the importance of the landscape connectivity in the heat island core patches from 2001 to 2021 was analyzed and quantified, with the following main findings:

(1) The surface urban heat island area in Xiamen from 2001 to 2021 shows a trend of rapid increase followed by gradual stabilization. Spatially, the rapidly developing southern main urban area and the south-central urban belt area around the bay are the main distribution areas of heat island patches, and the heat island morphology is gradually clear.

(2) The area of the heat island core category in the study area increased between 2011 and 2021, and there was a gradual tendency for the heat island cores to cluster. The six classes of edge, branch, islet, bridge, loop, and perforation had a small percentage of area, and all the above areas except for the perforation type showed a decreasing trend, so they had little impact on the urban thermal landscape. The above series of changes indicate that the urban construction program is biased towards a fixed concentration and the ecological protection of the areas outside the planning area.

(3) The key patches in the urban heat island network are still mainly located in the central part of the study area and their area has increased and they are more densely distributed. In the implementation of thermal mitigation measures, priority can be given to retrofitting the patches at the top of the importance value to obtain better mitigation effects.

(4) This study uses a combination of the MSPA graph theory approach and landscape connectivity modeling to create a heat island network to identify the key areas. Meanwhile, this study provides an effective thermal mitigation strategy from a network

perspective: destroying key patches in the heat island network to block the structural connectivity of the heat island network and connect it to cold islands.

(5) The organic combination of an MSPA analysis and landscape connectivity analysis can be applied to research related to urban heat islands and provide scientific guidance for urban development. However, in subsequent studies, it is necessary to construct a more refined and precise urban heat island network and identify its key nodes and channels in order to more effectively control the mitigation of the heat island effect under urbanization.

Author Contributions: Conceptualization, Z.C., J.D. and W.F.; methodology, Z.C., J.D. and W.F.; software, Z.C., X.L., M.L.,Y.C., Y.H. and T.L.; validation, Z.C., X.L., M.L., Y.C., Y.Z., J.C. and T.L.; formal analysis, Z.C., X.L. and Y.Z.; investigation, Z.C., M.L. and T.L.; resources, Z.C., X.L. and Y.H.; data curation, Z.C., X.L., M.L., Y.C., Y.H., Y.Z. and J.C.; writing—original draft preparation, Z.C., Y.H. and J.C.; writing—review and editing, Z.C., Y.C. and Y.Z.; visualization, Z.C., Y.C. and Y.H.; supervision, Z.C. and W.F.; project administration, J.D.; funding acquisition, J.D. and W.F. All authors have read and agreed to the published version of the manuscript.

Funding: This research was funded by (1) Unit: Ministry of Science and Technology of the People's Republic of China. Green Urbanization across China and Europe: Collaborative Research on Key Technological Advances in Urban Forests, grant number 2021YFE0193200; (2) Unit: Ministry of Science and Technology of the People's Republic of China. Horizon 2020 strategic plan: CLEARING HOUSE-Collaborative Learning in Research, Information sharing, and Governance on How Urban tree-based solutions support Sino-European urban futures, grant number 821242; (3) National Park Ecological Protection and High-quality Development Research Project, grant number KLE21013A.

Institutional Review Board Statement: Not applicable.

Informed Consent Statement: Not applicable.

Data Availability Statement: The data used to support the findings of this study are available from the corresponding author upon request.

Acknowledgments: We wish to thank the anonymous reviewers and editors for their detailed comments and suggestions.

Conflicts of Interest: The authors declare no conflict of interest.

References

1. Zhang, W.; Chang, W.J.; Zhu, Z.C.; Hui, Z. Landscape ecological risk assessment of Chinese coastal cities based on land use change. *Appl. Geogr.* **2020**, *117*, 102174. [CrossRef]
2. Liu, J.Y.; Kuang, W.H.; Zhang, Z.X.; Xu, X.L.; Qin, Y.W.; Ning, J.; Zhou, W.C.; Zhang, S.W.; Li, R.D.; Yan, C.Z.; et al. Spatiotemporal characteristics, patterns, and causes of land-use changes in China since the late 1980s. *J. Geogr. Sci.* **2014**, *24*, 195–210. [CrossRef]
3. Gong, J.; Yang, J.X.; Tang, W.W. Spatially Explicit Landscape-Level Ecological Risks Induced by Land Use and Land Cover Change in a National Ecologically Representative Region in China. *Int. J. Environ. Res. Public Health* **2015**, *12*, 14192–14215. [CrossRef] [PubMed]
4. Deng, J.S.; Wang, K.; Hong, Y.; Qi, J.G. Spatio-temporal dynamics and evolution of land use change and landscape pattern in response to rapid urbanization. *Landsc. Urban Plan.* **2009**, *92*, 187–198. [CrossRef]
5. Wang, M.; Liu, M.; Zhang, D.Q.; Qi, J.D.; Fu, W.C.; Zhang, Y.; Rao, Q.Y.; Bakhshipour, A.E.; Tan, S.K. Assessing and optimizing the hydrological performance of Grey-Green infrastructure systems in response to climate change and non-stationary time series. *Water Res.* **2023**, *232*, 119720. [CrossRef]
6. Qi, J.; He, B.-J.; Cao, Y.; Dong, J.; Lin, E.S. Risk assessment of terrestrial protected areas to extreme wind hazards: A case study in Queensland, Australia. *Landsc. Urban Plan.* **2023**, *240*, 104888. [CrossRef]
7. Tan, J.G.; Zheng, Y.F.; Tang, X.; Guo, C.Y.; Li, L.P.; Song, G.X.; Zhen, X.R.; Yuan, D.; Kalkstein, A.J.; Li, F.R.; et al. The urban heat island and its impact on heat waves and human health in Shanghai. *Int. J. Biometeorol.* **2010**, *54*, 75–84. [CrossRef]
8. He, B.J.; Wang, J.S.; Liu, H.M.; Ulpiani, G. Localized synergies between heat waves and urban heat islands: Implications on human thermal comfort and urban heat management. *Environ. Res.* **2021**, *193*, 110584. [CrossRef]
9. Deilami, K.; Kamruzzaman, M.; Liu, Y. Urban heat island effect: A systematic review of spatio-temporal factors, data, methods, and mitigation measures. *Int. J. Appl. Earth Obs. Geoinf.* **2018**, *67*, 30–42. [CrossRef]
10. Bao, J.Z.; Wang, Z.K.; Yu, C.H.; Li, X.D. The influence of temperature on mortality and its Lag effect: A study in four Chinese cities with different latitudes. *BMC Public Health* **2016**, *16*, 375. [CrossRef]

11. Adelaide, L.; Chanel, O.; Pascal, M. Health effects from heat waves in France: An economic evaluation. *Eur. J. Health Econ.* **2022**, *23*, 119–131. [CrossRef] [PubMed]
12. Mathew, A.; Khandelwal, S.; Kaul, N. Spatial and temporal variations of urban heat island effect and the effect of percentage impervious surface area and elevation on land surface temperature: Study of Chandigarh city, India. *Sustain. Cities Soc.* **2016**, *26*, 264–277. [CrossRef]
13. Cao, S.S.; Hu, D.Y.; Zhao, W.J.; Mo, Y.; Yu, C.; Zhang, Y. Monitoring changes in the impervious surfaces of urban functional zones using multisource remote sensing data: A case study of Tianjin, China. *GIScience Remote Sens.* **2019**, *56*, 967–987. [CrossRef]
14. Yu, Z.W.; Yang, G.Y.; Zuo, S.D.; Jorgensen, G.; Koga, M.; Vejre, H. Critical review on the cooling effect of urban blue-green space: A threshold-size perspective. *Urban For. Urban Green.* **2020**, *49*, 11. [CrossRef]
15. Chen, L.; Wang, X.L.; Cai, X.B.; Yang, C.; Lu, X.R. Combined Effects of Artificial Surface and Urban Blue-Green Space on Land Surface Temperature in 28 Major Cities in China. *Remote Sens.* **2022**, *14*, 448. [CrossRef]
16. Peng, J.; Xie, P.; Liu, Y.X.; Ma, J. Urban thermal environment dynamics and associated landscape pattern factors: A case study in the Beijing metropolitan region. *Remote Sens. Environ.* **2016**, *173*, 145–155. [CrossRef]
17. Chen, Y.J.; Yu, S.X. Impacts of urban landscape patterns on urban thermal variations in Guangzhou, China. *Int. J. Appl. Earth Obs. Geoinf.* **2017**, *54*, 65–71. [CrossRef]
18. Zhang, Y.; Wang, Y.C.; Ding, N. Spatial Effects of Landscape Patterns of Urban Patches with Different Vegetation Fractions on Urban Thermal Environment. *Remote Sens.* **2022**, *14*, 5684. [CrossRef]
19. Yao, L.; Li, T.; Xu, M.X.; Xu, Y. How the landscape features of urban green space impact seasonal land surface temperatures at a city-block-scale: An urban heat island study in Beijing, China. *Urban For. Urban Green.* **2020**, *52*, 12. [CrossRef]
20. Masoudi, M.; Tan, P.Y. Multi-year comparison of the effects of spatial pattern of urban green spaces on urban land surface temperature. *Landsc. Urban Plan.* **2019**, *184*, 44–58. [CrossRef]
21. Du, H.Y.; Cai, Y.L.; Zhou, F.Q.; Jian, H.; Jiang, W.Y.; Xu, Y.Q. Urban blue-green space planning based on thermal environment simulation: A case study of Shanghai, China. *Ecol. Indic.* **2019**, *106*, 11. [CrossRef]
22. Qi, J.D.; Lin, E.S.; Tan, P.Y.; Ho, R.C.M.; Sia, A.; Olszewska-Guizzo, A.; Zhang, X.D.; Waykool, R. Development and application of 3D spatial metrics using point clouds for landscape visual quality assessment. *Landsc. Urban Plan.* **2022**, *228*, 14. [CrossRef]
23. Yu, Z.W.; Guo, X.Y.; Jorgensen, G.; Vejre, H. How can urban green spaces be planned for climate adaptation in subtropical cities? *Ecol. Indic.* **2017**, *82*, 152–162. [CrossRef]
24. Shih, W.Y. Greenspace patterns and the mitigation of land surface temperature in Taipei metropolis. *Habitat Int.* **2017**, *60*, 69–80. [CrossRef]
25. Zhou, W.Q.; Wang, J.; Cadenasso, M.L. Effects of the spatial configuration of trees on urban heat mitigation: A comparative study. *Remote Sens. Environ.* **2017**, *195*, 1–12. [CrossRef]
26. Li, X.M.; Zhou, W.Q.; Ouyang, Z.Y. Relationship between land surface temperature and spatial pattern of greenspace: What are the effects of spatial resolution? *Landsc. Urban Plan.* **2013**, *114*, 1–8. [CrossRef]
27. Yu, Z.W.; Zhang, J.U.; Yang, G.Y.; Schlaberg, J. Reverse Thinking: A New Method from the Graph Perspective for Evaluating and Mitigating Regional Surface Heat Islands. *Remote Sens.* **2021**, *13*, 1127. [CrossRef]
28. Wang, S.; Wu, M.Q.; Hu, M.M.; Fan, C.; Wang, T.; Xia, B.C. Promoting landscape connectivity of highly urbanized area: An ecological network approach. *Ecol. Indic.* **2021**, *125*, 107487. [CrossRef]
29. Qian, W.Q.; Li, X.Y. A cold island connectivity and network perspective to mitigate the urban heat island effect. *Sustain. Cities Soc.* **2023**, *94*, 104525. [CrossRef]
30. Wang, F.; Wang, Y.W. Potential role of local contributions to record-breaking high-temperature event in Xiamen, China. *Weather Clim. Extrem.* **2021**, *33*, 100338. [CrossRef]
31. Jimenez-Munoz, J.C.; Sobrino, J.A.; Skokovic, D.; Mattar, C.; Cristobal, J. Land Surface Temperature Retrieval Methods from Landsat-8 Thermal Infrared Sensor Data. *IEEE Geosci. Remote Sens. Lett.* **2014**, *11*, 1840–1843. [CrossRef]
32. Yang, J.; Sun, J.; Ge, Q.S.; Li, X.M. Assessing the impacts of urbanization-associated green space on urban land surface temperature: A case study of Dalian, China. *Urban For. Urban Green.* **2017**, *22*, 1–10. [CrossRef]
33. Fan, H.Y.; Yu, Z.W.; Yang, G.Y.; Liu, T.Y.; Liu, T.Y.; Hung, C.H.; Vejre, H. How to cool hot-humid (Asian) cities with urban trees? An optimal landscape size perspective. *Agric. For. Meteorol.* **2019**, *265*, 338–348. [CrossRef]
34. Yu, X.L.; Guo, X.L.; Wu, Z.C. Land Surface Temperature Retrieval from Landsat 8 TIRS-Comparison between Radiative Transfer Equation-Based Method, Split Window Algorithm and Single Channel Method. *Remote Sens.* **2014**, *6*, 9829–9852. [CrossRef]
35. Zhao, H.B.; Zhang, H.; Miao, C.H.; Ye, X.Y.; Min, M. Linking Heat Source-Sink Landscape Patterns with Analysis of Urban Heat Islands: Study on the Fast-Growing Zhengzhou City in Central China. *Remote Sens.* **2018**, *10*, 1268. [CrossRef]
36. Soille, P.; Vogt, P. Morphological segmentation of binary patterns. *Pattern Recognit. Lett.* **2009**, *30*, 456–459. [CrossRef]
37. Lin, J.Y.; Qiu, S.X.; Tan, X.J.; Zhuang, Y.Y. Measuring the relationship between morphological spatial pattern of green space and urban heat island using machine learning methods. *Build. Environ.* **2023**, *228*, 109910. [CrossRef]
38. Vogt, P.; Ferrari, J.R.; Lookingbill, T.R.; Gardner, R.H.; Riitters, K.H.; Ostapowicz, K. Mapping functional connectivity. *Ecol. Indic.* **2009**, *9*, 64–71. [CrossRef]
39. Taylor, P.D.; Fahrig, L.; Henein, K.; Merriam, G. Connectivity Is a Vital Element of Landscape Structure. *Oikos* **1993**, *68*, 571–573. [CrossRef]

40. Pascual-Hortal, L.; Saura, S. Integrating landscape connectivity in broad-scale forest planning through a new graph-based habitat availability methodology: Application to capercaillie (*Tetrao urogallus*) in Catalonia (NE Spain). *Eur. J. For. Res.* **2008**, *127*, 23–31. [CrossRef]
41. Kindlmann, P.; Burel, F. Connectivity measures: A review. *Landsc. Ecol.* **2008**, *23*, 879–890. [CrossRef]
42. Yu, Z.W.; Yao, Y.W.; Yang, G.Y.; Wang, X.R.; Vejre, H. Spatiotemporal patterns and characteristics of remotely sensed region heat islands during the rapid urbanization (1995–2015) of Southern China. *Sci. Total Environ.* **2019**, *674*, 242–254. [CrossRef] [PubMed]
43. Yu, Z.W.; Zhang, J.G.; Yang, G.Y. How to build a heat network to alleviate surface heat island effect? *Sustain. Cities Soc.* **2021**, *74*, 103135. [CrossRef]
44. An, Y.; Liu, S.L.; Sun, Y.X.; Shi, F.N.; Beazley, R. Construction and optimization of an ecological network based on morphological spatial pattern analysis and circuit theory. *Landsc. Ecol.* **2021**, *36*, 2059–2076. [CrossRef]
45. Wei, Q.Q.; Halike, A.; Yao, K.X.; Chen, L.M.; Balati, M. Construction and optimization of ecological security pattern in Ebinur Lake Basin based on MSPA-MCR models. *Ecol. Indic.* **2022**, *138*, 108857. [CrossRef]
46. Hao, X.M.; Li, W.H. Oasis cold island effect and its influence on air temperature: A case study of Tarim Basin, Northwest China. *J. Arid Land* **2016**, *8*, 172–183. [CrossRef]
47. Lai, D.Y.; Liu, W.Y.; Gan, T.T.; Liu, K.X.; Chen, Q.Y. A review of mitigating strategies to improve the thermal environment and thermal comfort in urban outdoor spaces. *Sci. Total Environ.* **2019**, *661*, 337–353. [CrossRef]
48. Mohajerani, A.; Bakaric, J.; Jeffrey-Bailey, T. The urban heat island effect, its causes, and mitigation, with reference to the thermal properties of asphalt concrete. *J. Environ. Manag.* **2017**, *197*, 522–538. [CrossRef]
49. Akbari, H.; Kolokotsa, D. Three decades of urban heat islands and mitigation technologies research. *Energy Build.* **2016**, *133*, 834–842. [CrossRef]
50. Qi, J.D.; Ding, L.; Lim, S. A Decision-Making Framework to Support Urban Heat Mitigation by Local Governments. *Resour. Conserv. Recycl.* **2022**, *184*, 106420. [CrossRef]
51. Qi, J.D.; Ding, L.; Lim, S. Application of a decision-making framework for multi-objective optimisation of urban heat mitigation strategies. *Urban Clim.* **2023**, *47*, 101372. [CrossRef]